

13. P. A. Thompson and G. S. Grest, *Phys. Rev. Lett.* **67**, 1751 (1991).
 14. J. M. Carlson and J. S. Langer, *ibid.* **62**, 2632 (1989).
 15. S. J. Hirz *et al.*, *Langmuir* **8**, 328 (1992).
 16. W. B. Russel, D. A. Saville, W. R. Schowalter, *Colloidal Dispersions* (Cambridge Univ. Press, Cambridge, 1989), chap. 14.
 17. H. M. Jaeger and S. R. Nagel, *Science* **255**, 1523 (1992).
 18. H. A. Barnes, J. F. Hutton, K. Walters, *An Introduction to Rheology* (Elsevier, Amsterdam, 1989); R. L. Hoffman, *J. Colloid Interface Sci.* **46**, 491 (1974).
 19. M. O. Robbins and P. A. Thompson, personal communication.
 20. J. N. Israelachvili, *Intermolecular and Surface*

Forces (Academic Press, London, ed. 2, 1991).
 21. Y. L. Chen, C. Helm, J. N. Israelachvili, *J. Phys. Chem.* **95**, 10736 (1991).
 22. F. P. Bowden and D. Tabor, *Friction and Lubrication* (Methuen, London, 1967), chap. 9.
 23. B. J. Briscoe, D. C. B. Evans, D. Tabor, *J. Colloid Interface Sci.* **61**, 9 (1977).
 24. Y. L. Chen *et al.*, *J. Phys. Chem.* **93**, 7057 (1989).
 25. Y. L. Chen, H. Yoshizawa, J. Israelachvili, unpublished results.
 26. M. Suzuki, Y. Saotome, M. Yanagisawa, *Thin Solid Films* **160**, 453 (1988).
 27. E. Ando *et al.*, *ibid.* **180**, 287 (1989).
 28. B. J. Ackerson and N. A. Clarke, *Physica A* **118**,

221 (1983); W. Xue and G. S. Grest, *Phys. Rev. Lett.* **64**, 419 (1990); M. J. Stevens, M. O. Robbins, J. F. Belak, *ibid.* **66**, 3004 (1991).
 29. G. Bireshaw, *Tribology and the Liquid-Crystalline State*, ACS Symposium Series No. 441 (American Chemical Society, Washington, DC, 1990).
 30. A. M. Bibo, C. M. Knobler, I. R. Peterson, *J. Phys. Chem.* **95**, 5591 (1991).
 31. Supported by the U.S. Department of Energy and Exxon Chemicals. We thank S. Banerjee, G. Fredrickson, S. Granick, J. Langer, G. Leal, D. Pearson, M. Robbins, and P. Thompson for insightful comments and discussions.

29 June 1992; accepted 30 November 1992

Three-Dimensional Instabilities of Mantle Convection with Multiple Phase Transitions

S. Honda, D. A. Yuen, S. Balachandar, D. Reuteler

The effects of multiple phase transitions on mantle convection are investigated by numerical simulations that are based on three-dimensional models. These simulations show that cold sheets of mantle material collide at junctions, merge, and form a strong downflow that is stopped temporarily by the transition zone. The accumulated cold material gives rise to a strong gravitational instability that causes the cold mass to sink rapidly into the lower mantle. This process promotes a massive exchange between the lower and upper mantles and triggers a global instability in the adjacent plume system. This mechanism may be cyclic in nature and may be linked to the generation of superplumes.

Phase transitions in the mantle may affect the amount of flow between the upper and lower mantles (1, 2). Recently, the effects of phase transitions on mantle convection have been studied with the use of numerical models (3–7), but most have been restricted to two dimensions. Some interesting phenomena, such as the intermittently layered convection that is enforced by the spinel-to-perovskite phase transition (3–5), have been shown in these studies. The generation of diapirs in the upper mantle has also been demonstrated (4). Three-dimensional (3-D) studies are needed to confirm these interesting 2-D findings. Seismic tomographic studies (8, 9) have indicated that slabs may be lying horizontally along the phase transition zone. Investigations in two dimensions (4, 6, 7) have also shown the importance of including the second phase transition, olivine to spinel, at a depth of 400 km. In this report, we present results from 3-D numerical simulations of mantle convection with both major phase transitions and discuss an instability

in convection that is produced by the phase transitions. This instability may help ex-

plain the correlation between subduction rate changes and the superplume events (10) that occurred 120 million years ago and led to the unusually rapid production of the oceanic crust and the stabilization of the polarity of the Earth's magnetic field. The instability bears no resemblance to local boundary-layer instabilities that are seen in models of convection without phase changes. This global instability, which is produced by phase transitions, was first observed in 2-D models (6, 7), but these 3-D simulations have confirmed their existence.

The model that we used is based on a Cartesian geometry with an aspect ratio of 5 by 5 by 1, with unity being the depth of the layer. A mantle depth of 2000 km is assumed in which the two major

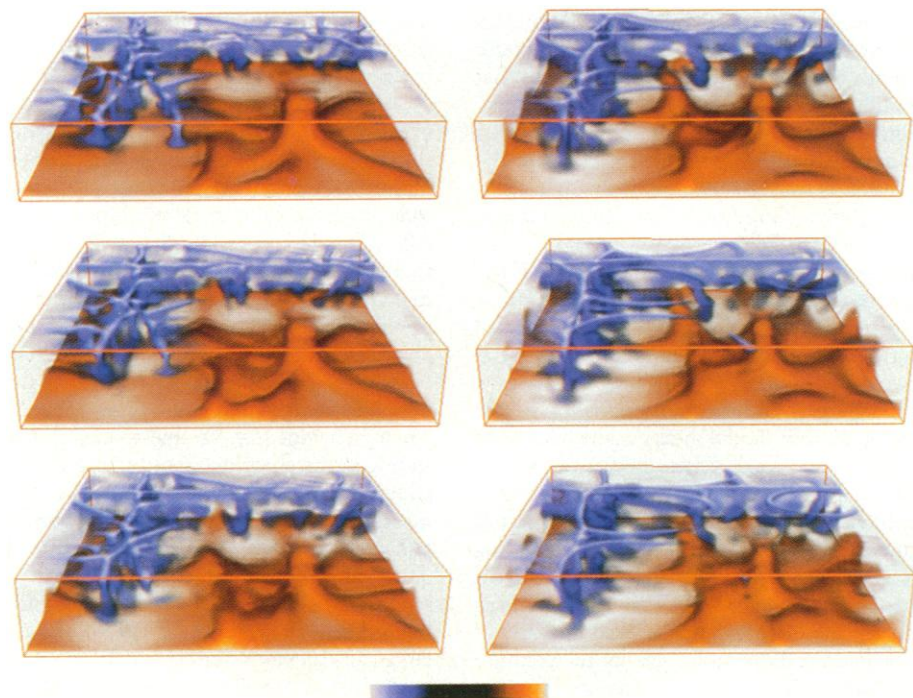


Fig. 1. Sequence of snapshots of temperature T . Sequence of events begins with the top left panel, goes down the column and continues with the right column, going down at equal time intervals. The first and last frames represent $t = 0.010$ (1.270 billion years) and $t = 0.0125$ (1.588 billion years). Cold and hot anomalies have been volume-rendered in blue and yellow hues, respectively, as indicated by the color bar. The void represents values close to the average value of 0.5. The aspect ratio of this 3-D box is 5 by 5 by 1.

S. Honda, Department of Earth and Planetary Systems Science, University of Hiroshima, Higashi-Hiroshima 724, Japan.

D. A. Yuen and D. Reuteler, Minnesota Supercomputer Institute and Department of Geology and Geophysics, University of Minnesota, Minneapolis, MN 55415.

S. Balachandar, Department of Theoretical and Applied Mechanics, University of Illinois, Urbana, IL 61801.

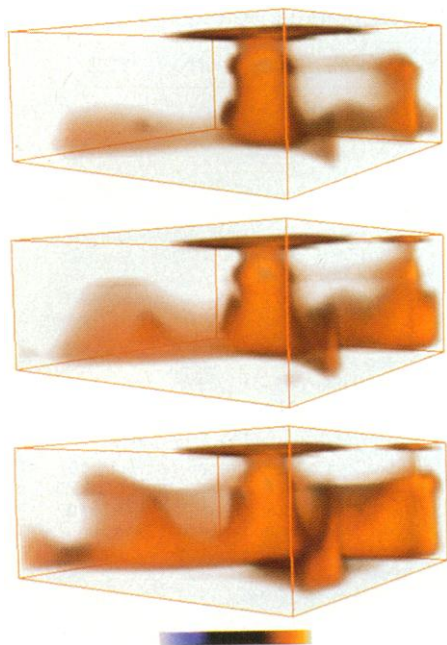


Fig. 2. Closer view of the development of plume dynamics. Only the hot thermal anomalies are shown with the same temperature cutoff of 0.5. Times range from $t = 1.334$ billion to 1.461 billion years at equal intervals.

phase transitions are located at depths of 400 and 670 km. The Cartesian geometry allows sufficient resolution for the capture of the complicated dynamics at the transition zones. Comparison of 2-D Cartesian and axisymmetrical spherical models (4–7) indicates that the effects of sphericity on the local dynamics of the upper-mantle phase changes are not large. Plumes can also be simulated to greater precision at the phase-transitional depths

(3) with Cartesian geometry because the radii of curvature of the Earth and those associated with phase changes differ by only 10%.

We used the extended Boussinesq approximation (6, 7, 11, 12) to model 3-D mantle convection with a thermal expansivity $\alpha(z)$ (13), an exponentially increasing viscosity $\eta(z)$, and a thermal conductivity $\kappa(z)$, all of which depend on depth (14). This approximation has been shown in 2-D simulations to yield results (15) similar to those of the compressible anelastic equations. To handle the sharp changes in the buoyancy forces and latent heat release at the transition zone, we used a formalism based on an effective thermal expansivity (6, 7, 11, 12). In this treatment, the thermal expansivity α consists of two parts: the first prescribes the background variations that result from the overburden pressure (13), and the second is localized in nature and describes the sharp variations of α across the phase change zone (6, 7, 11, 12). The use of an effective depth-dependent thermal expansivity instead of a complete treatment that accounts for phase boundary distortion considerably reduces the computation time (11, 12, 16).

The dimensionless equations for the balance of mass momentum and energy, in terms of velocity \mathbf{u} , temperature T , and dynamical pressure p , under the extended Boussinesq assumption (17) are used in this simulation. These equations assume an infinite Prandtl number, as is appropriate for mantle convection, and have been nondimensionalized, which is appropriate for a slow viscous flow (17). The dimensionless parameters Di_T (dissipation number) and

Ra_T (Rayleigh number) are based on surface values (18).

The total thermal expansivity $\alpha(z)$ is given by

$$\alpha(z) = \alpha_b(z) + \alpha_1(z) + \alpha_2(z) \quad (1)$$

where $\alpha_b(z)$ is attributable to the overburden pressure and takes on the functional dependence extrapolated from experimental data (19) and the localized functions $\alpha_1(z)$ and $\alpha_2(z)$ represent, respectively, the olivine-to-spinel and the spinel-to-perovskite phase changes (20). Using the experimental data for these two transitions (21, 22), we made the assumption that the absolute values of the Clapeyron slopes are equal (23) for both transitions but that the olivine-to-spinel transition is exothermic and the spinel-to-perovskite transition is endothermic. Viscosity is assumed to vary by a factor of 10 (24), and the thermal conductivity increases with depth by a factor of ~ 4 (19, 25). The equations of motion (17) include the effects of density changes across the phase boundaries in the momentum equation and latent heat effects in the energy equation. They are integrated in time with a fully spectral method (26).

The simulation was started from an initial condition with no phase change and $Ra_T = 2 \times 10^6$. This was run for 25,600 time steps, which corresponds to 3.25 billion years. Visualization of 3-D temperature fields (27) plays an important role in this endeavor. In time-dependent convection, there is a strong interaction between the descending flows and ascending plumes. In Fig. 1, we show six snapshots of the volume-rendered T fields in an interval of time between $t = 0.010$ and 0.0125, which corresponds to

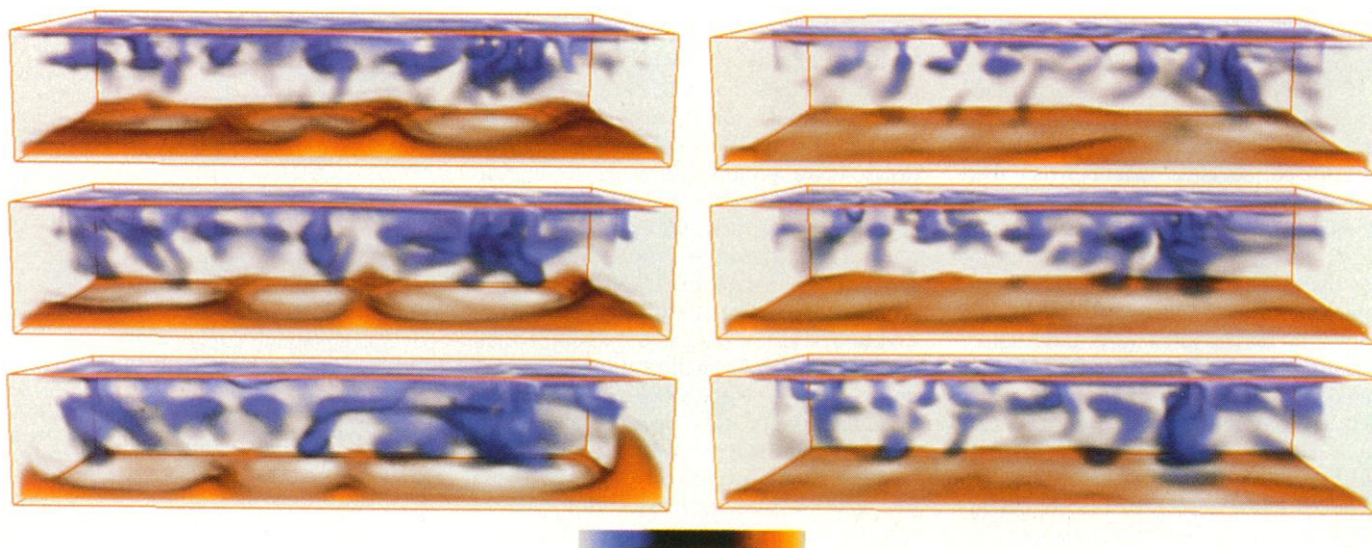


Fig. 3. A close side view of the temperature fields of the cold material. The time span of the left three panels ranges from $t = 1.270$ billion to 1.429 billion years in equal increments. The right three panels cover the last stages from $t = 2.025$ billion to 3.253 billion years in equal increments.

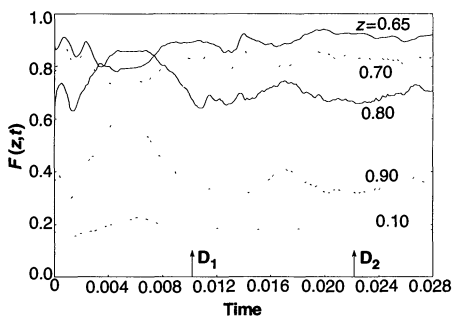


Fig. 4. Normalized vertical mass flux $F(z,t)$ for five depths. The depths associated with the spinel-to-perkovite and the olivine-to-spinel transitions correspond to, respectively, $z = 0.65$ and $z = 0.8$. The time interval spans 3.253 billion years. The normalized vertical mass flux is defined in (6) and is the root-mean-square vertical velocity at a given depth divided by the global kinetic energy. The arrows D_1 and D_2 represent the onset of the two flushing events.

times of 1.270 billion and 1.588 billion years from the initial state.

Large cylindrical plumes (yellow), which are found in convection without phase transitions (11, 12), are produced by the depth-dependent thermal expansivity and viscosity from a focusing effect (11, 12). These upwellings penetrate the phase boundaries, but their stems thin as they do so. Mushroom-like heads appear near the surface. A network of interconnected cold sheets (blue), which do not all penetrate the transition zone, is observed. These downwellings differ in appearance from the sharp descending sheets that are seen in the case without phase change (11, 12).

In our simulation, cold material accumulates at a junction. Over time, this process results in a large gravitational instability. Eventually there is a rapid discharge of upper-mantle cold material into the lower mantle [starting at the second frame ($t = 1.334$ billion years) and ending a frame later ($t = 1.398$ billion years)]. This rapid dump of cold material causes a strong lateral flow at the bottom of the mantle, which then causes the plume system to go into a convulsive mode and produce widespread heating (Fig. 1, right-hand column). In the meantime, the original instability associated with the flushing of cold material ceases, and the sinking currents are once again hindered by the phase changes. Cold material begins to accumulate in the transition zone again, which will give rise to another unstable episode.

In Fig. 2, we show the lateral temperature fields, $\delta T(x,y,z,t)$ (28) to better demonstrate the lateral thermal anomalies. This quantity is useful for visualizing complex plume structures. The rapid rise of the plumes during the instability period is quite striking. Some of the weaker ones are de-

flected by the phase transitions (Fig. 2, left background). A close-up of the cold descending flows during the entire period shows that the cold material is rebuilding in the transition zone (Fig. 3, left panels) and flushes again (Fig. 3, right panels).

Time series of the vertical mass flux $F(z,t)$ (29) for five different depths are shown in Fig. 4. The maximum in the curve that corresponds to the depth of the olivine-to-spinel transition ($z = 0.8$) marks the layered period. This is followed by a sharp drop (D_1), which is the peak of the avalanche event in which all of the cold material is focused into the junction and horizontal motion dominates. Below this transition in the upper mantle, the magnitudes of the vertical velocity are considerably larger, especially at the level of the spinel-to-perovskite transition ($z = 0.65$). This suggests that the olivine-to-spinel transition can help trigger the instability. On the other hand, in the deep mantle ($z = 0.1$), the vertical flow is subdued because of the depth-dependent properties (11, 12).

During the instability, the cold downwelling current pulls massive amounts of material with it because of the large reservoir of material that builds up in the transition zone. Thus, cold material can reach the bottom much easier than in the case without any phase change (11, 12). A similar finding has been reported for a spherical model with the endothermic phase change (30). This result may shed some light on the lower-mantle tomographic results (31) in that it suggests that fast anomalies in the lower mantle may reflect the presence of subduction sites in the past.

Many other factors in the mantle can influence the generation of this instability. One is the temperature dependence of viscosity: cold material lingers in the transition zone longer because of its intrinsically higher viscosity. Thus, the instability would be more dramatic because a larger reservoir would form before it would be dumped. Internal heating from radioactive decay helps promote layering in mantle convection (32); this greater tendency to layer means a greater ability to store a cold pool in the transition zone, which would generate an instability. Likewise, the soft rheological zone beneath the spinel-to-perovskite transition (33) would also enhance the mechanical decoupling of the lower and upper mantles, which would encourage the accumulation of cold material above the spinel-to-perovskite transition.

Superplume events (10) in the past might be a consequence of this type of mega-instability that is produced by the periodic formation of cold pools in the transition zone. Such phenomena may still occur if the convective vigor of the mantle is still potent enough for cold material to

accumulate in the transition zone (31).

REFERENCES AND NOTES

1. F. A. Vening-Meinesz, *Proc. K. Ned. Akad. Wet.* **B59**, 1 (1956).
2. J. Verhoogen, *Philos. Trans. R. Soc. London Ser. A* **258**, 276 (1965).
3. M. Liu, D. A. Yuen, W. Zhao, S. Honda, *Science* **252**, 1836 (1991).
4. P. Machetel and P. Weber, *Nature* **350**, 55 (1991).
5. W. R. Peltier and L. P. Solheim, *Geophys. Res. Lett.* **19**, 321 (1992).
6. V. Steinbach and D. A. Yuen, *ibid.*, p. 2243.
7. D. A. Yuen, U. Hansen, W. Zhao, A. P. Vincent, A. V. Malevsky, *J. Geophys. Res.*, in press.
8. R. van der Hilst, R. Engdahl, W. Spakman, G. Nolet, *Nature* **353**, 37 (1991).
9. Y. Fukao, M. Obayashi, H. Inoue, M. Nishii, *J. Geophys. Res.* **97**, 4809 (1992).
10. R. L. Larson, *Geology* **19**, 547 (1991); _____ and P. L. Olson, *Earth Planet. Sci. Lett.* **107**, 437 (1991). There was a high rate of production of oceanic plateaus, seamount chains, and continental flood basalts between 120 million and 75 million years ago in the Pacific.
11. U. R. Christensen and D. A. Yuen, *J. Geophys. Res.* **90**, 10291 (1985).
12. S. Balachandar, D. A. Yuen, D. Reuteler, *Geophys. Res. Lett.* **19**, 2247 (1992).
13. A. Chopelas and R. Boehler, *ibid.* **16**, 1347 (1989).
14. M. Osako and E. Ito, *ibid.* **18**, 239 (1991). The thermal conductivity of mantle material increases with pressure. A factor of 4 increase across the mantle was extrapolated from the above laboratory work.
15. V. Steinbach, U. Hansen, A. Ebel, *ibid.* **16**, 633 (1989).
16. The effects of phase boundary distortion have not been included here. Consideration would require the addition of equations that describe the motions of the phase boundaries [see (5, 11, 12)]. Christensen and Yuen (11) found that the effective thermal expansivity approximation describes well the strictly layered or single-layered regimes by comparing the two approaches. Differences become greater in the intermediate region between the two end-members. Computational time would have increased enormously if we had included phase boundary distortion. Seismic data [P. M. Shearer and T. G. Masters, *Nature* **355**, 791 (1992)] indicate that the amplitude of the seismic-discontinuity distortion is ~ 30 km.
17. For fluids with an infinite Prandtl number, we nondimensionalized the time with the use of the thermal diffusion time across the layer. A time interval of 127 million years corresponds to a nondimensional time of 0.001. Velocity is nondimensionalized by κ/H , where κ is taken here to be $10^{-6} \text{ m}^2 \text{ s}^{-1}$ and H , the layer depth, is 2000 km. The temperature has been nondimensionalized with respect to the temperature difference across the mantle, taken here to be 2500 K. The partial differential equations governing \mathbf{u} , T , and p can be found in (12). The temporal evolution is governed only by the conservation of energy.
18. The dissipation number Di_T and Rayleigh number Ra_T are based on surface values. The value of Di_T is taken to be 0.5, and Ra_T is taken to be 2×10^6 , which is about a factor of 5 smaller than realistic estimates for the mantle. The value of Di_T decreases by a factor of about 4 across the mantle, whereas Ra_T decreases by a factor of about 160 because of the combined depth variations of thermal expansivity, viscosity, and thermal conductivity.
19. Background thermal expansivity decreases with density according to $1/\rho^6$, as determined experimentally by Chopelas and Boehler (13). In the extended Boussinesq approximation, ρ is a constant, and the depth dependence of α follows

$$\alpha(z) = \alpha_0 \left[1 + 2 \frac{Di_1}{\gamma T} (1-z) \right]^{-3}$$

with $\gamma_T = 1.4$.

20. The localized contributions to α are due to phase transitions. The functional form that is assumed is $A_i \exp[(z - z_i)/\sigma]^2$ with z_i being 0.65 and 0.80, respectively, for the spinel to perovskite and the olivine to spinel phase changes and $\sigma = 0.02$, which corresponds to a phase transition width of 40 km. The constant A_i is given in (6, 7, 11, 12) and depends on the density change across the transition, the Clapeyron slope, background thermal expansivity, gravity, mean density, and the depth of the mantle. For the olivine-to-spinel and spinel-to-perovskite transitions, the values of A_i that we used were, respectively, 5 and -5. The sign of the Clapeyron slope determines the degree of local enhancement or decrease of the overall thermal expansivity. This localized α is regarded as a simplification because the effects of phase boundary distortion and change in width of the transition zone are not accounted for.
21. E. Ito and E. Takahashi, *J. Geophys. Res.* **94**, 10637 (1989); R. Boehler and A. Chopelas, *Geophys. Res. Lett.* **18**, 1147 (1991).
22. T. Katsura and E. Ito, *J. Geophys. Res.* **94**, 15663 (1989); A. Chopelas, *ibid.* **96**, 11817 (1991).
23. The magnitudes of the Clapeyron slopes for the olivine-to-spinel and spinel-to-perovskite transitions are between 2.5 and 3.0 M Pa K^{-1} (21, 22). Phase changes are assumed to occur under equilibrium situations, and sluggish kinetic effects in cold descending flows are not considered.
24. There are many ways to parameterize the depth variations of mantle viscosity. An exponential dependence is based on the effect of activation volume in the mantle-creep laws [see, for example, G. Ranalli, *Rheology of the Earth* (Allen and Unwin, London, 1987)].
25. The phonon contribution to the thermal conductivity goes as p^4 [D. L. Anderson, *Phys. Earth Planet. Inter.* **45**, 307 (1987)].
26. S. Balachandar and D. A. Yuen, *J. Comput. Phys.*, in press. Periodic boundary conditions are imposed along the sides, and the boundary conditions at the top and bottom are stress free, impermeable, and at different constant temperatures. There is no internal heating. We used a Fourier-Chebyshev spectral expansion with 70 grid points in the vertical and 100 in the horizontal direction. We used a coordinate stretching [A. Bayliss and E. Turkel, *J. Comput. Phys.* **101**, 349 (1992)] in the vertical direction to better resolve the local dynamics. Examination of the spectral decay of the temperature and velocity components in the vertical and two horizontal directions show decay over several orders in magnitude, which indicates adequate spatial resolution of the smallest relevant length scales in all three directions. The time step of about 10^{-6} that corresponds to CFL numbers of 0.3 to 0.4 is much smaller than the smallest time scales of the flow.
27. K. Chin-Purcell, in "Workshop on Visualization and Statistical Analysis in Hard Turbulence," in Minnesota Supercomputer Institute Research Report, USMI 92/189, Minneapolis (1992). BOB (Brick of Bytes) is an interactive program for volume rendering of 3-D data on a Silicon Graphics work station.
28. S. Honda, *J. Phys. Earth* **35**, 195 (1987). The temperature increment $\delta T = T - \langle T \rangle$, where the angle brackets denote an average over the horizontal plane.
29. Normalized vertical mass flux is a ratio between the root-mean-square vertical velocity over a plane and the root-mean-square velocity [see (6)].
30. P. Tackley, D. J. Stevenson, G. Glatzmaier, G. Schubert, *Nature*, in press.
31. W. Su and A. M. Dziewonski, *Phys. Earth Planet. Inter.* **74**, 29 (1993). H. Inoue, Y. Fukao, K. Tanabe, Y. Ogata, *ibid.* **59**, 294 (1990).
32. W. Zhao, D. A. Yuen, S. Honda, *ibid.* **72**, 185 (1992).
33. S.-I. Karato and P. Li, *Science* **255**, 1238 (1992). This softening in rheology is attributable to the change of crystal structure in perovskite.
34. We thank V. Steinbach, W. Zhao, R. Boehler, U. R. Christensen, and P. Tackley for discussions. This research has been supported by the Geochemistry program at National Science Foundation, National Aeronautics and Space Administration, and the von Humboldt Stiftung of Germany. S.H. was the recipient of a visiting scholar grant from the Minnesota Supercomputer Institute.

4 November 1992; accepted 17 December 1992

Toward a Model for the Interaction Between Elongation Factor Tu and the Ribosome

Albert Weijland and Andrea Parmeggiani

In the elongation cycle of bacterial protein synthesis the interaction between elongation factor-Tu (EF-Tu)-guanosine triphosphate (GTP), aminoacyl-transfer RNA (aa-tRNA), and messenger RNA-programmed ribosomes is associated with the hydrolysis of GTP. This interaction determines the selection of the proper aa-tRNA for incorporation into the polypeptide. In the canonical scheme, one molecule of GTP is hydrolyzed in the EF-Tu-dependent binding of aa-tRNA to the ribosome, and a second molecule is hydrolyzed in the elongation factor-G (EF-G)-mediated translocation of the polypeptide from the ribosomal A site to the P site. Substitution of Asp¹³⁸ with Asn in EF-Tu changed the substrate specificity from GTP to xanthosine triphosphate and demonstrated that the EF-Tu-mediated reactions involved the hydrolysis of two nucleotide triphosphates for each Phe incorporated. This stoichiometry of two is associated with the binding of the correct aa-tRNA to the ribosome.

Elongation factor-Tu (EF-Tu) of *Escherichia coli* is a guanine nucleotide-binding protein that functions as the carrier of aminoacyl-tRNA (aa-tRNA) to the ribosome in protein synthesis (1). In the past 25 years the stoichiometry of guanosine triphos-

phate (GTP) hydrolysis and peptide bond formation has been investigated repeatedly, but despite these efforts no conclusive results have been obtained (2-4). A stoichiometry of two GTP molecules hydrolyzed was derived from the evidence that EF-Tu and elongation factor-G (EF-G) each bind one molecule of GTP and that EF-Tu, GTP, and aa-tRNA form a trimeric com-

plex. One of the GTP molecules hydrolyzed was associated with the EF-Tu-dependent binding of aa-tRNA to the ribosome prior to peptide bond formation, the other with the EF-G-mediated translocation of the polypeptide chain from the ribosomal A site to the P site, which occurs after the incorporation of a new amino acid residue. Higher stoichiometries obtained from a complete translation system were attributed to guanosine triphosphatase (GTPase) activities uncoupled from protein biosynthesis (4). Recently, Ehrenberg *et al.* (5) reopened this problem by proposing on the basis of kinetic studies that two molecules of GTP are hydrolyzed by EF-Tu for each phenylalanine incorporated. Accordingly, the carrier of aa-tRNA to the ribosomes would not be a trimeric complex but a pentameric complex containing two EF-Tu molecules. Intermolecular interactions of EF-Tu had already been suggested on the basis of genetic (6) and biochemical evidence (7), but only for a combination of two EF-Tu mutants. The proposed pentameric model remains controversial. Biochemical and physical-chemical experiments have recently supported the existence of a trimeric complex (8).

In order to assess in the complete elongation cycle the precise stoichiometry of the EF-Tu-aa-tRNA-ribosome interaction, we selected a method that avoids some of the inherent difficulties—that both elongation factors are GTPases, that the EF-G GTPase activity is stimulated by ribosomes in the absence of protein synthesis, and that even highly purified ribosomal preparations include nonspecific nucleotidases. Protein synthesis is complex even in a simplified *in vitro* system, and determination of stoichiometry requires correction factors that are difficult to measure accurately. Therefore, we distinguished EF-Tu-dependent GTP hydrolysis from EF-G and other ribosomal GTPases with a mutant EF-Tu in which substitution of Asp¹³⁸ with Asn (EF-Tu D138N) changed the substrate specificity from GTP to xanthosine triphosphate (XTP). This change was predicted from the three-dimensional model of EF-Tu (or the related model of *H-ras* p21) in which Asp¹³⁸ (or Asp¹¹⁹ in p21) interacts with the exocyclic 2-amino group of the purine ring of GTP (9). Hwang and Miller, using a maxi-cell system have reported that EF-Tu D138N forms a stable complex with XTP, aa-tRNA, and ribosomes (10). Because maxicells yield only small amounts of EF-Tu D138N and these are contaminated by the wild-type elongation factor, we constructed and expressed the plasmid-borne EF-Tu D138N in *E. coli* and purified the protein product to homogeneity, completely free from EF-Tu wild type (11).

In the presence of XTP purified EF-Tu

SDI n° 61840 du Centre National de la Recherche Scientifique, Laboratoire de Biochimie, Ecole Polytechnique, F-91128 Palaiseau Cedex, France.